Tunable fiber-tip lens based on thermo-optic effect of amorphous silicon

Ping Li (李 平), Jing Liu (刘 静), Peng Huang (黄 鹏), Xingyu Zhang (张星宇), Jinhui Shi (史金辉)*, Libo Yuan (苑立波), and Chunying Guan (关春颖)**

Key Laboratory of In-Fiber Integrated Optics of Ministry of Education, College of Science, Harbin Engineering University, Harbin 150001, China

**Corresponding author: shijinhui@hrbeu.edu.cn; **corresponding author: cyguan@163.com*

Received October 12, 2019; accepted December 11, 2019; posted online March 6, 2020

We theoretically demonstrate a compact all-dielectric metasurface fiber-tip lens composed of sub-wavelength amorphous silicon on the end face of a multimode fiber. The full 2π phase control was realized by varying the widths of resonant units. The tunable focal length is achieved by using the thermal-optic effect of amorphous silicon. The focal length increases from 309 μm to 407 μm when the temperature changes by 300 K. The temperature controlled all-fiber integrated lens is compact and with high efficiency and provides an excellent platform of a fiber-tip lab. Meanwhile, the proposed fiber lens does not have any structural changes during dynamic tuning, which improves the durability and repeatability of the devices.

Keywords: fiber-tip lens; tunable focus length; all-dielectric metasurface; thermal-optic effect.
doi: 10.3788/COL202018.030602.

Plasmonic metasurfaces have low transmission efficiencies due to intrinsic metal loss. In contrast, all-dielectric resonant metasurfaces avoid absorption losses and can enhance the transmission efficiency. The all-dielectric metasurface has become a new trend in the metasurface field in recent years[1–7]. The dielectric metasurfaces based on high refractive index dielectric material such as silicon[1–3], phase-change material[4–6], and titanium dioxide[7–9] have demonstrated that they can achieve various electromagnetic responses as metallic counterparts[10–12], which provides new opportunities to improve the efficiencies and performance of metasurface devices. All-dielectric metasurface refers to an ultra-thin two-dimensional (2D) structure that is composed of periodic dielectric resonators, which can efficiently manipulate the electromagnetic characteristics of electromagnetic waves such as the phase, amplitude, polarization, and transmission mode[13–15]. The traditional convex lens controls the wave front by changing the thickness of the lens to form a curved shape[16]. However, due to low refractive indices of conventional optical materials, a bulky thickness is usually required to achieve the full 2π control of the phase, and the miniaturization of optical devices is too difficult to achieve. A metalens, an ultra-thin planar lens based on a metasurface, is miniature and with high quality. The focal length tuning over a wide range is urgently required in cameras, cellphones, and other wearable mobile devices[17,18]. Recently, reported tunable focusing metalenses were mostly achieved by deformation flexibility of elastic materials, which can produce a steerable deformation under external mechanical or electrical stimuli[19–21]. Although these methods can provide a wide-range focal length modulation, additional mechanical or electrode structures increase the difficulty of the design and fabrication and also limit the miniaturization of optical devices. Due to small size, long-distance transmission, and flexibility, the optical fiber offers an excellent platform for achieving micro–nano optical devices[22–26]. The fiber-based integrated system can greatly simplify the operating procedures of optical devices and reduce the size of the optical systems since they do not require strict spatial alignment and coupling optical path. Meanwhile, it can also eliminate the influence of oblique incidence of the light on device performance.

In this work, we demonstrate a tunable all-dielectric metasurface lens based on a fiber tip, where sub-wavelength amorphous silicon units are designed on the end face of a multimode fiber. The focal length of the metasurface lens can be tuned by changing the temperature due to the high thermal-optic coefficient of amorphous silicon. The temperature controlled all-fiber metasurface lens is compact and with high efficiency and can interconnect with conventional optical fiber systems. Meanwhile, the proposed fiber-tip lens will not have any structural changes during dynamic tuning, which improves the durability and repeatability of the devices. The proposed lens is integrated on the fiber end, greatly reducing the size of the focusing lens system.

The single mode fiber is difficult to achieve high-efficiency focusing due to the small size of the core, which limits the number of the attached resonators. However, the multimode fiber has a large core size and core end, and thus it can support a large number of resonators, so high-efficiency focusing based on multimode fiber-tip integration can be achieved. The lateral view diagram of the all-dielectric fiber lens is shown in Fig. 1(a). The resonators with constant width ($w = 1$ μm) composed of amorphous silicon are arranged on the end face of the multimode optical fiber. The resonators can be fabricated on the fiber tip by a micromachining technology[27]. The high thermo-optic effect of the amorphous silicon is used

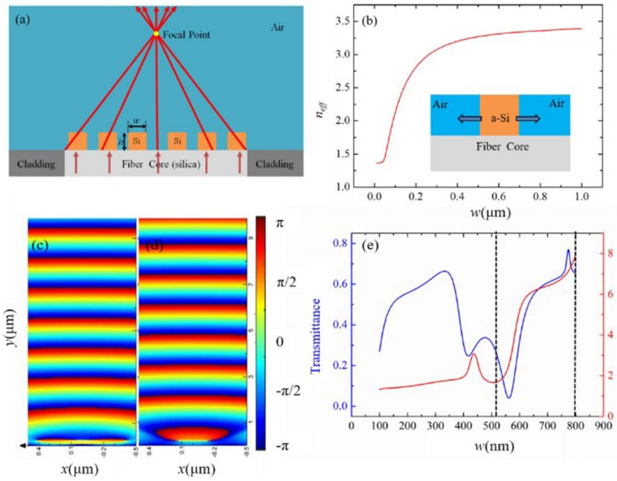

Fig. 1. (a) Schematic of the all-dielectric fiber-tip lens. (b) The effective refractive index of a single resonator as a function of the width of silicon. Phase distributions of the resonators with the silicon widths of (c) 500 nm and (d) 600 nm. (e) The changes of the phase delay and transmittance of the resonator as a function of the width of silicon. The width of the silicon resonators of the optimized fiber-tip lens is chosen between two black dotted lines.

to modulate the refractive index of the amorphous silicon and achieve dynamic control of the focal length. The thermo-optic coefficient of amorphous silicon film can reach the order of 2.3×10^{-4} within the near-infrared wavelength range at room temperature (300 K)[28,29]. As the light from the multimode fiber core is incident into a single resonator, the phase delay depends on the height h, width w, and refractive index n_{si} of the silicon elements. In order to simplify the calculation of fiber integrated devices, the propagation properties of the resonator unit cell and lens are investigated using the 2D finite-difference time-domain method (FDTD, Lumerical FDTD Solutions). In reality the nanoscale concentric dielectric ring resonators are distributed on the fiber end face. The change of effective refractive index caused by the spatial arrangement of the resonators can enable phase delay modulation in the range from 0 to 2π. In the simulation, the wavelength λ is 1300 nm, the height of the resonators is fixed at 400 nm, and the period of the resonators is 1 μm; the refractive indexes of the amorphous silicon and the fiber core are $n_{\text{si}} = 3.5226$[30] and $n_{\text{core}} = 1.4579$, respectively. Figure 1(b) shows the relationship between the effective refractive index of the single resonator and the width of silicon. When the period of the resonators is constant, the effective refractive index initially increases rapidly and then slowly approaches its asymptote with the increasing width of the silicon unit; therefore, the variable silicon resonators could be used to achieve the full 2π phase modulation. The phase distributions introduced by the resonator with the silicon widths of 500 nm and 600 nm are shown in Figs. 1(c) and 1(d), where the height of the resonator is 400 nm. The phase delay between the two resonators is approximately π at the same propagation distance. The phase delay and the transmittance of the single resonator are shown in Fig. 1(e) for varying width w of silicon. When the width w is changed from 500 to 800 nm, the resonator can achieve an ideal phase delay in the range from 0 to 2π, and the phase delay increases with the increasing width of the resonator. The changes of the phase delay and the transmittance are attributed to the electric and magnetic dipole resonances in the single resonator. If the space between two adjacent silicon resonators is too small, near-field coupling will occur, and the strong interaction between them will affect the transmission phase distributions, as a result increasing the difficulty in the device design. In order to avoid near-field coupling and reduce the difficulty of the fabrication, the width of silicon is selected in the range from 500 nm to 800 nm [the region between two black lines in Fig. 1(e)], and the aspect ratio of the silicon resonator unit is 0.5–0.8.

The aperture D of the designed all-dielectric fiber-tip lens is 50 μm, and the lens contains 48 resonators. To achieve the focal length f, the phase function $\phi(x)$ on the fiber end is required to satisfy the following formula:

$$\phi(x) = \frac{2\pi f}{\lambda} - \frac{2\pi\sqrt{f^2 + x^2}}{\lambda} + 2m\pi. \tag{1}$$

The phase distributions on the fiber end for different focal lengths are shown in Fig. 2(a). The phase function becomes flat as the focal length becomes larger for the same operating wavelength. The phase delay increases with the increase of the focal length at the same x-axis position, which is more obvious when the position is closer to the edge of the fiber-tip lens. Linearly polarized Gaussian light polarized perpendicularly to the x–y plane was launched from the core of the multimode fiber upon the all-dielectric metasurface lens. In the simulation, the length of the multimode fiber is 2 μm. Figure 2(b) shows the calculated electric field intensity distribution of the focusing beam at room temperature of 300 K. The focal length is about ~309 μm and agrees well with the designed value of 300 μm. The electric field intensity along the x direction at the focus spot ($y = 309$ μm) is displayed in Fig. 2(c). The full width at half-maximum (FWHM) of the focus spot is about 9 μm. The transmittance of the fiber-tip lens is 46.6%. The simulation results show that the all-dielectric metasurface based on the multimode fiber tip can achieve the focusing performance.

The refractive index of the amorphous silicon can be modulated due to its high thermo-optic effect, so the dynamic manipulation of the focal length can be achieved. Here, the thermo-optic coefficient of the fiber core and cladding can be ignored due to the tiny change of the refractive index of silica in the considered temperature range. The field intensities of the all-dielectric fiber-tip lens at different temperatures are shown in Fig. 3. The focal length changes from 309 μm to 407 μm when the temperature increases from room temperature to 600 K. The relationship between the focal length and the temperature

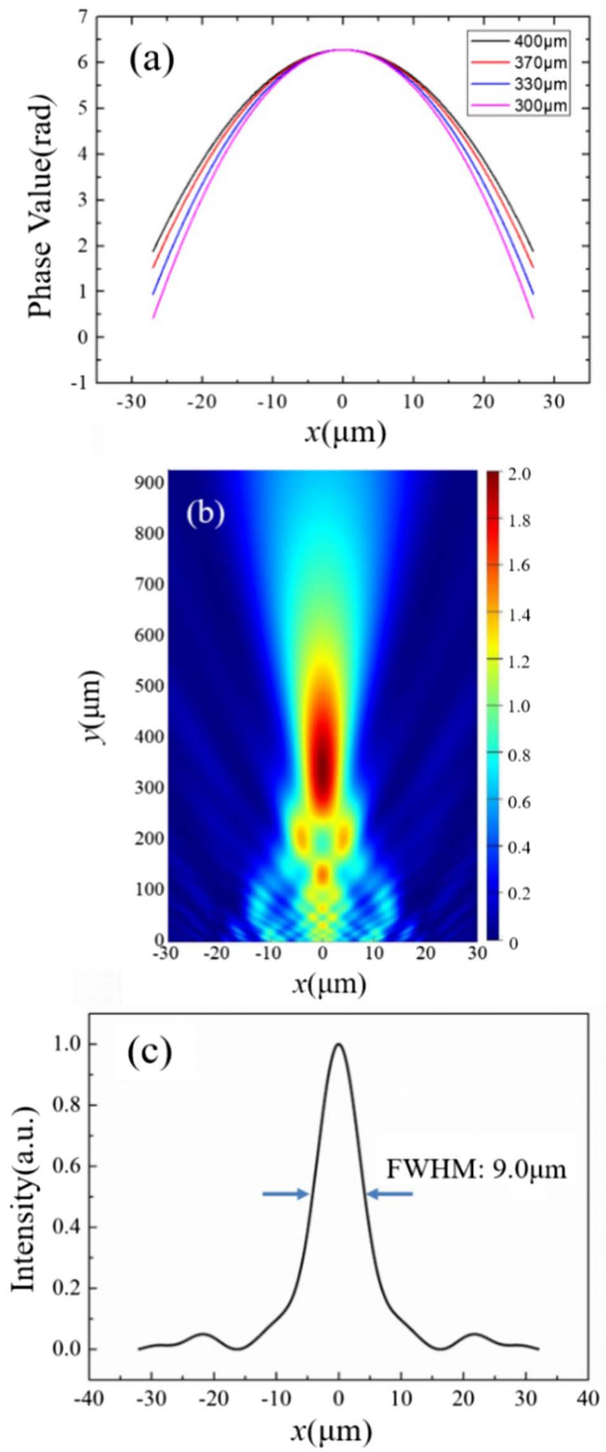

Fig. 2. (a) Phase distributions for different focal lengths (1300 nm). (b) The field intensity distribution of the fiber-tip lens with the focal length of ~309 μm. The color bar indicates the electric field intensity. (c) Normalized electric field intensity distribution of the fiber-tip lens along the x axis at the focal plane ($y = 309$ μm). The FWHM is 9.0 μm.

is depicted by a yellow dashed line. The temperature sensitivity S of the focal length is approximately 0.33 μm/K. The figure of merit (FOM), which is defined as the ratio between the tuning of focal length S and focal length f, is 0.11 K^{-1} ($\mathrm{FOM} = S/f$). The electric field

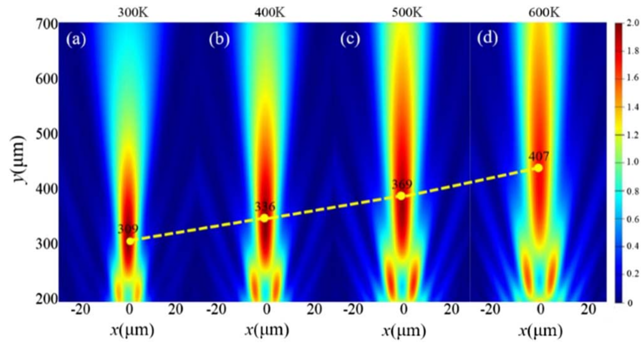

Fig. 3. Change of focal lengths of the fiber lens for different temperatures.

intensities along the y direction ($x = 0$ μm) are displayed in Fig. 4(a). Obviously, the depth of focus of the focusing beam along the y direction increases with the temperature. Figure 4(b) shows the normalized electric field intensity distributions of the fiber-tip lens along the x axis at the focal length. The FWHMs of the focus spots are 9.0 μm, 9.5 μm, 11.6 μm, and 10.2 μm for the temperatures of 300 K, 400 K, 500 K, and 600 K, respectively, approaching the value calculated by the diffraction limit formula,

$$d = 1.22\frac{\lambda f}{D}, \tag{2}$$

where the aperture D is equal to the size of the fiber-tip all-dielectric metasurface. The FWHM of the focus spot increases by 1 μm in the temperature range of 300 K. The good focus effect can always be maintained as the temperature varies. The absolute focusing efficiency of the fiber-tip lens is ~30% for different temperatures, as shown in Fig. 4(c).

In conclusion, a compact tunable all-dielectric multimode fiber-tip lens based on the high thermo-optic effect of amorphous silicon was demonstrated. The rectangular amorphous silicon nanoresonators were arranged on the end face of a multimode fiber to construct an all-dielectric metasurface lens. By varying the width of resonators, the full 2π phase control was realized. The tunable range of the focal length is up to 100 μm when the temperature changes in the range of 300 K. The multimode interference in the multimode fiber can be avoided by splicing a piece of multimode fiber with the single mode fiber to form an end cap. The temperature controlled all-fiber integrated lens is compact and with high efficiency and provides an excellent platform for realizing the fiber-tip lab. Meanwhile, the proposed fiber lens does not have any structural changes during dynamic tuning, which improves the durability and repeatability of the devices. In addition, the proposed fiber-tip lens does not require strict spatial alignment and coupling optical path, which greatly simplifies the operating procedures of optical devices and reduces the size of the optical systems.

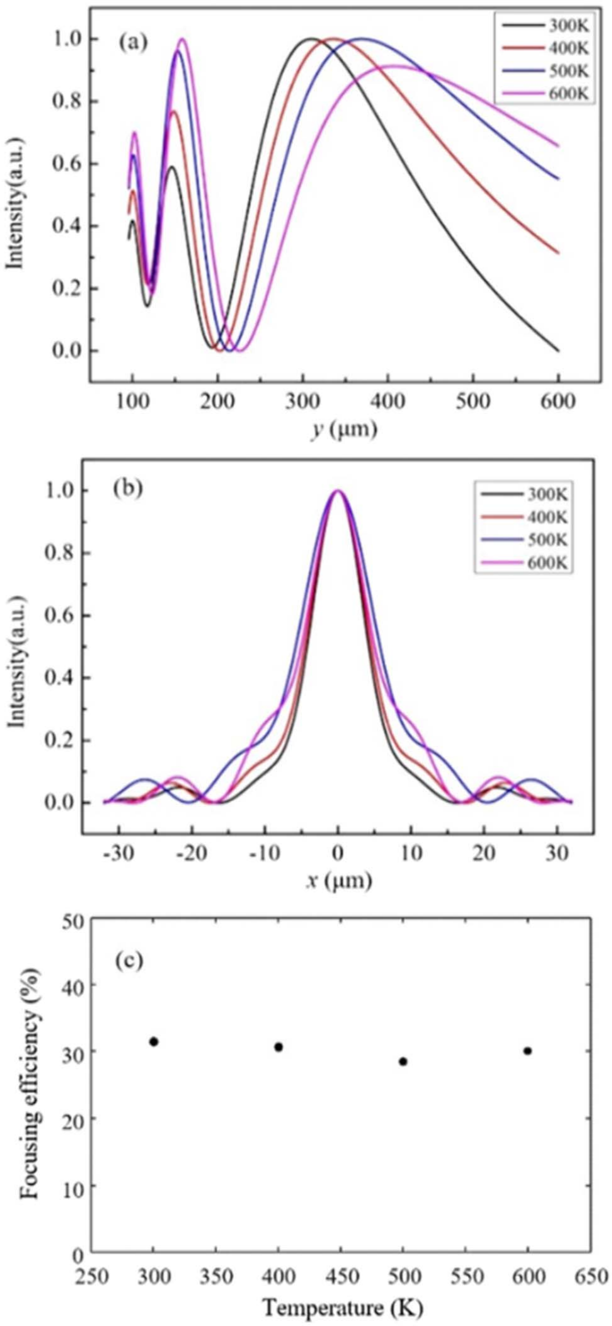

Fig. 4. Normalized electric field intensity distributions of the fiber-tip lens (a) along the y direction ($x = 0$ μm) and (b) along the x axis at the focal length for different temperatures. (c) The focusing efficiency of the fiber-tip lens.

This work was supported by the National Natural Science Foundation of China (NSFC) (Nos. 91750107, 61675054, 61875044, and U1931121), the Natural Science Foundation of Heilongjiang Province in China (No. ZD2018015), 111 Project of the Harbin Engineering University (No. B13015), and the Fundamental Research Funds for the Central Universities (Nos. 3072019CF2501, 3072019CF2521, and 3072019CF2509).

References

1. J. Proust, F. Bedu, B. Gallas, I. Ozerov, and N. Bonod, ACS Nano **10**, 7761 (2016).
2. Z. Zhou, J. Li, R. Su, B. Yao, H. Fang, K. Li, L. Zhou, J. Liu, D. Stellinga, C. P. Reardon, T. F. Krauss, and X. Wang, ACS Photon. **4**, 544 (2017).
3. D. Sell, J. Yang, S. Doshay, K. Zhang, and J. A. Fan, ACS Photon. **3**, 1919 (2016).
4. Q. Wang, E. T. F. Rogers, B. Gholipour, C. Wang, G. Yuan, J. Teng, and N. I. Zheludev, Nat. Photon. **10**, 60 (2016).
5. A. V. Pogrebnyakov, J. A. Bossard, J. P. Turpin, J. D. Musgraves, H. J. Shin, C. Rivero-Baleine, N. Podraza, K. A. Richardson, D. H. Werner, and T. S. Mayer, Opt. Mater. Express **8**, 2264 (2018).
6. C. Choi, S. J. Kim, J. G. Yun, J. Sung, S. Y. Lee, and B. Lee, Chin. Opt. Lett. **16**, 050009 (2018).
7. P. Gutruf, C. Zou, W. Withayachumnankul, M. Bhaskaran, S. Sriram, and C. Fumeaux, ACS Nano **10,** 133 (2015).
8. S. Sun, Z. Zhou, C. Zhang, Y. Gao, Z. Duan, S. Xiao, and Q. Song, ACS Nano **11**, 4445 (2017).
9. M. Khorasaninejad, W. T. Chen, R. C. Devlin, J. Oh, A. Y. Zhu, and F. Capasso, Science **352**, 1190 (2016).
10. J. Lee, M. Tymchenko, C. Argyropoulos, P. Y. Chen, F. Lu, F. Demmerle, G. Boehm, M. C. Amann, A. Alù, and M. A. Belkin, Nature **511**, 65 (2014).
11. F. Ding, Z. Wang, S. He, V. M. Shalaev, and A. V. Kildishev, ACS Nano **9**, 4111 (2015).
12. F. Qin, L. Ding, L. Zhang, F. Monticone, C. C. Chum, J. Deng, S. Mei, Y. Li, J. Teng, M. Hong, S. Zhang, A. Alù, and C. W. Qiu, Sci. Adv. **2**, e1501168 (2016).
13. A. Arbabi, Y. Horie, M. Bagheri, and A. Faraon, Nat. Nanotechnol. **10**, 937 (2015).
14. S. Jahani and Z. Jacob, Nat. Nanotechnol. **11**, 23 (2016).
15. M. I. Shalaev, J. Sun, A. Tsukernik, A. Pandey, K. Nikolskiy, and N. M. Litchinitser, Nano Lett. **15**, 6261 (2015).
16. D. C. O'Shea, T. J. Suleski, A. D. Kathman, and D. W. Prather, *Diffractive Optics: Design, Fabrication, and Test* (SPIE, 2004).
17. T. B. Pittman, Y. H. Shih, D. V. Strekalov, and A. V. Sergienko, Phys. Rev. A **52**, R3429 (1995).
18. S. Colburn, A. Zhan, and A. Majumdar, Optica **5**, 825 (2018).
19. S. M. Kamali, E. Arbabi, A. Arbabi, Y. Horie, and A. Faraon, Laser Photon. Rev. **10**, 1002 (2016).
20. A. She, S. Zhang, S. Shian, D. R. Clarke, and F. Capasso, Sci. Adv. **4**, eaap9957 (2018).
21. E. Arbabi, A. Arbabi, S. M. Kamali, Y. Horie, M. Faraji-Dana, and A. Faraon, Nat. Commun. **9**, 812 (2018).
22. T. Gissibl, S. Thiele, A. Herkommer, and H. Giessen, Nat. Commun. **7**, 11763 (2016).
23. N. Yu and F. Capasso, J. Lightwave Technol. **33**, 2344 (2015).
24. G. H. Yuan, E. T. F. Rogers, and N. I. Zheludev, Light: Sci. Appl. **6**, e17036 (2017).
25. M. Principe, M. Consales, A. Micco, A. Crescitelli, G. Castaldi, E. Esposito, V. L. Ferrara, A. Cutolo, V. Galdi, and A. Cusano, Light: Sci. Appl. **6**, e16226 (2017).
26. J. Wang, Chin. Opt. Lett. **16**, 050006 (2018).
27. M. Khorasaninejad, F. Aieta, P. Kanhaiya, M. A. Kats, P. Genevet, D. Rousso, and F. Capasso, Nano Lett. **15**, 5358 (2015).
28. F. G. Della Corte, M. E. Montefusco, L. Moretti, and I. Rendina, Appl. Phys. Lett. **79,** 168 (2001).
29. M. Iodice, G. Mazzi, and L. Sirleto, Opt. Express **14**, 5266 (2006).
30. D. T. Pierce and W. E. Spicer, Phys. Rev. B **5**, 3017 (1972).